


Article

Wireless Battery Charging Circuit Using Load Estimation without Wireless Communication

Sang-Won Lee ¹, Yoon-Geol Choi ², Jung-Ha Kim ¹ and Bongkoo Kang ^{1,*}

¹ Department of Electrical Engineering, Pohang University of Science and Technology, Pohang, Kyungpook 37673, Korea; sangwony1@postech.ac.kr (S.-W.L.); jungaha@postech.ac.kr (J.-H.K.)

² LS Industrial Systems R&D Campus, LS-ro 116 beongil 40, Dongan-gu, Anyang-si, Gyeonggi-do 14118, Korea; ygchoi2@lsis.com

* Correspondence: bkkang@postech.ac.kr; Tel.: +82-54-279-5939

Received: 15 October 2019; Accepted: 21 November 2019; Published: 25 November 2019



Abstract: A wireless battery charging circuit is proposed, along with a new load estimation method. The proposed estimation method can predict the load resistance, mutual inductance, output voltage, and output current without any wireless communication between the transmitter and receiver sides. Unlike other estimation methods that sense the high-frequency AC voltage and current of the transmitter coil, the proposed method only requires the DC output value of the peak current detection circuit at the transmitter coil. The proposed wireless power transfer (WPT) circuit uses the estimated parameters, and accurately controls the output current and voltage by adjusting the switching phase difference of the transmitter side. The WPT prototype circuit using a new load estimation method was tested under various coil alignment and load conditions. Finally, the circuit was operated in a constant current and constant voltage modes to charge a 48-V battery pack. These results show that the proposed WPT circuit that uses the new load estimation method is well suited for charging a battery pack.

Keywords: wireless power transfer (WPT) circuit; battery charger; load estimation; constant current (CC) charging; constant voltage (CV) charging

1. Introduction

Wireless power transfer (WPT) technologies have been rapidly developed and widely applied to many industrial applications, such as biomedical devices, consumer electronics, manufacturing facilities, and electric vehicles (Evs), where direct contact between power supplies and applications is impossible or inconvenient [1–4]. To efficiently transfer power, most of the WPT circuits use electromagnetic coupling between coils. These WPT circuits use capacitors to reduce reactive power [5–13], and can be largely categorized into four types, depending on whether the capacitors are connected with the transmitter and receiver coils in series and series (S-S), series and parallel (S-P), parallel and parallel (P-P), or parallel and series (P-S) [5–7]. Among them, the S-S circuit has been widely used because the capacitances can be chosen independently of the load and coupling conditions [7–10].

A typical S-S WPT circuit (Figure 1) [7,9,10] consists of a full-bridge inverter (Q_1 – Q_4), a transmitter coil (L_1), a full-bridge rectifier (D_1 – D_4), a receiver coil (L_2), and two capacitors (C_1 and C_2). L_1 forms a resonance circuit with C_1 , and L_2 forms a resonance circuit with C_2 . Both resonance circuits are designed to have the same resonance frequency $\omega_o = 2\pi \cdot f_o = 1/\sqrt{L_1 C_1} = 1/\sqrt{L_2 C_2}$. The transmitter and receiver coils have a mutual inductance, M_{12} . The input to the full-bridge inverter is a DC voltage V_{DC} .

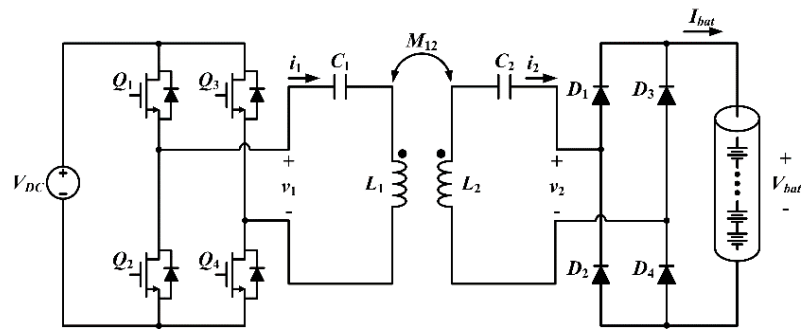


Figure 1. The series and series (S-S) wireless power transfer (WPT) circuit for charging a battery.

To charge a battery, the S-S WPT circuit should be operated in constant current (CC) output mode when the battery voltage V_{bat} is lower than predetermined limit voltage $V_{bat,cut}$, and in constant voltage (CV) mode when $V_{bat,cut} \leq V_{bat} < \text{charging voltage limit (CVL)}$ [[9–12]. To support both modes, an additional DC–DC converter can be inserted between the S-S WPT circuit and the battery. However, the additional converter decreases the power transfer efficiency η_e and the power density [8,13]. To solve this problem, the battery can be directly connected to the S-S WPT circuit, as in Figure 1, and several control methods have been introduced [9–13].

The WPT circuit in [9] uses the same S-S WPT circuit (Figure 1) and adopts a pulse frequency modulation (PFM) method to obtain a CV output. In this circuit, the switching frequency range should be selected differently whenever the coupling coefficient is varied, so the range of the frequency limiter cannot be determined easily when the coupling coefficient k_{12} varies widely. Also, wireless communication should be introduced to operate the PFM method. The circuit in [10] improves η_e by using two intermediate coils that are placed between the transmitter and receiver coils, and uses $f = f_{CC}$ for CC output and $f = f_{CV}$ for CV output, where the frequencies f_{CC} and f_{CV} are determined by the coupling coefficients among the four coils. However, the values of f_{CC} and f_{CV} vary in the manner that any coupling coefficient varies, and no method has been developed to date to measure the coupling coefficients, so accurate determination of f_{CC} and f_{CV} is a difficult task. The circuits in [11,12] use auxiliary switches and capacitors to change the output from CC to CV mode. However, this circuit needs wireless communication to change the operational mode, and additional components also decrease the power density. As mentioned above, most of control methods require wireless communication to know the load conditions and coupling state.

To eliminate the necessity for wireless communication, several load estimation methods have been presented [14–19]. The methods in [14–16] predict the load resistance R_L by using the information of the input voltage and current. However, these methods should know the value of the coupling state before estimating the load conditions, so they cannot be used for various coil alignments. The method in [17] adopts an additional capacitor in the S-S WPT circuit; this method operates the circuit in two modes for system identification, and analyzes the reflected impedance. However, the additional capacitor and bidirectional switch increase the circuit cost. The method in [18] measures the input voltage and current, and separates the imaginary part of the input impedance. To estimate the load conditions and coupling state, this method is implemented at one frequency, which is not a resonant frequency, so the impedance of the resonant tank slightly decreases the power transfer efficiency. The method in [19] injects a high frequency energy into the S-S WPT circuit, then detects the response of the circuit to estimate the load conditions. However, this method cannot follow the load conditions after initial energy injection. All of these methods [14–19] can estimate the load conditions well, so they should be able to sense the high-frequency AC input voltage and current. The resonant frequency of the WPT circuit can be up to several hundred kilohertz, so the sampling frequency should be much higher than the resonant frequency; as a result, the analog-to-digital conversion is difficult.

This paper proposes a wireless battery charging circuit along with a load estimation method. This circuit does not need any wireless communication between the transmitter and receiver sides,

and predicts the load resistance R_L , output voltage V_{bat} , output current I_{bat} , and mutual inductance M_{12} . In addition, because the simple peak current detection circuit is applied at the transmitter coil, the proposed circuit only senses the DC value, and does not need a high sampling frequency. The proposed WPT circuit senses the peak current values of the transmitter coil at f_o and auxiliary frequency f_a , and calculates the load conditions by using these values. Then, the proposed WPT circuit operates in CC and CV modes, depending on the estimated load conditions and phase shift control of the full-bridge inverter. In Section 2, the analysis of the proposed WPT circuit with a load estimation method is given based on the fundamental harmonic approximation (FHA), experimental results are presented in Section 3, possible errors in the proposed estimation method are analyzed in Section 4, and a conclusion is given in Section 5.

2. Wireless Power Transfer Circuit for Battery Charging

2.1. Theoretical Models of the S-S WPT Circuit

The gate control pulses Q_{g1} – Q_{g4} (Figure 2) for the full-bridge inverter have a switching frequency $f = 1/T = \omega/(2\pi)$. The switching phase of Q_{g1} and \bar{Q}_{g2} lags behind that of Q_{g3} lags behind that of \bar{Q}_{g4} by an angle ϕ , so the bipolar output pulses of the full-bridge inverter (v_1 , Figure 2) have a dead phase angle ϕ between the pulses. The fundamental component of v_1 is given by

$$v_1(t) = V_1 \sin(\omega t) = \frac{2V_{DC}}{\pi}(1 + \cos \phi) \sin(\omega t). \quad (1)$$

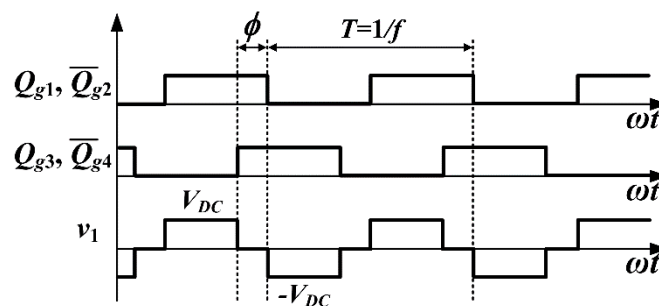


Figure 2. The gate signals and output voltage v_1 of the full-bridge inverter.

The current $i_1(t)$ of the transmitter coil, the current $i_2(t)$ of the receiver coil, and the input voltage $v_2(t)$ to the rectifier in Figure 1 can be expressed as

$$i_1 = I_1 \sin(\omega t + \theta) \quad (2)$$

$$v_2(t) = V_2 \sin(\omega t + \theta + \phi) = \frac{4V_{bat}}{\pi} \sin(\omega t + \theta + \phi) \quad (3)$$

$$i_2(t) = I_2 \sin(\omega t + \theta + \phi) = \frac{I_{bat}\pi}{2} \sin(\omega t + \theta + \phi), \quad (4)$$

where θ and ϕ are phase angles, V_{bat} is the battery voltage, and I_{bat} is the averaged charging current of the battery.

The S-S WPT circuit had an equivalent circuit (Figure 3) for the fundamental component, where R_{in} , R_1 , and R_2 are the equivalent series resistances (ESRs) of the full-bridge inverter, primary coil, and secondary coil, respectively. Using Equations (3) and (4), the equivalent resistance of the battery R_{bat} can be modeled with an equivalent resistance $R_{L,eq}$ as:

$$R_{L,eq} = \frac{8}{\pi^2} \cdot R_{bat} = \frac{8}{\pi^2} \cdot \frac{V_{bat}}{I_{bat}}. \quad (5)$$

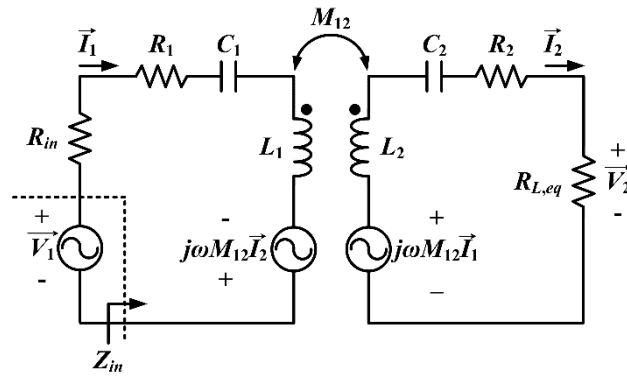


Figure 3. Equivalent circuit for the S-S WPT circuit. R_{in} , R_1 , and R_2 are equivalent series resistances of the full-bridge inverter, primary coil, and secondary coil, respectively.

Then, the Kirchhoff's voltage law (KVL) gives

$$\vec{V}_1 = (R_{in} + Z_1) \vec{I}_1 - j\omega M_{12} \vec{I}_2, \quad (6)$$

$$j\omega M_{12} \vec{I}_1 = (Z_2 + R_{L,eq}) \vec{I}_2, \quad (7)$$

where $Z_1 = R_1 + j\omega L_1 + 1/(j\omega C_1)$ and $Z_2 = R_2 + j\omega L_2 + 1/(j\omega C_2)$. Using Equations (6) and (7), the phase of the input impedance Z_{in} (Figure 4a), the voltage conversion ratio T_v (Figure 4b), the amplitude of $i_1(t)$, the peak current of $i_1(t)$ (I_1) (Figure 4c), the amplitude of $i_2(t)$, and the peak current of $i_2(t)$ (I_2) (Figure 4d) are calculated as

$$\vec{Z}_{in} = \frac{\vec{V}_1}{\vec{I}_1} = \frac{(R_{in} + Z_1)(Z_2 + R_{L,eq}) + \omega^2 M_{12}^2}{Z_2 + R_{L,eq}}, \quad (8)$$

$$T_v = \left| \frac{\vec{V}_2}{\vec{V}_1} \right| = \left| \frac{R_{L,eq} \vec{I}_2}{\vec{V}_1} \right| = \left| \frac{j\omega M_{12} R_{L,eq}}{(R_{in} + Z_1)(Z_2 + R_{L,eq}) + \omega^2 M_{12}^2} \right|, \quad (9)$$

$$I_1 = \left| \frac{Z_2 + R_{L,eq}}{(R_{in} + Z_1)(Z_2 + R_{L,eq}) + \omega^2 M_{12}^2} \right| \cdot V_1, \quad (10)$$

$$I_2 = \left| \frac{j\omega M_{12}}{(R_{in} + Z_1)(Z_2 + R_{L,eq}) + \omega^2 M_{12}^2} \right| \cdot V_1. \quad (11)$$

2.2. Load Estimation Method Using the Magnitude of Input Impedance

The proposed circuit uses the simple peak detection circuit (Figure 5) in [20] to measure the peak current of the transmitter coil I_1 as a DC value. The peak detection circuit is composed of a current sensor, an amplifier for the peak detection (A_1), an amplifier for the voltage follower (A_2), an input resistance of peak detector (R_i), a feedback loop resistance (R_f), a feedback loop diode (D_f), a rectification diode (D_o), an output capacitor (C_o), and an output resistance (R_o). If the output voltage of the current sensor (V_s) is lower than the voltage of C_o (V_o), D_f remains on, and D_o remains off. In this operating mode, the output voltage of A_2 (V_{out}) is clamped to V_o , and C_o is discharged by R_o . When V_o becomes smaller than V_s , D_f is turned off and D_o is turned on. In this operating mode, C_o is charged to the new positive peak of V_s , so $V_s = V_o = V_{out}$.

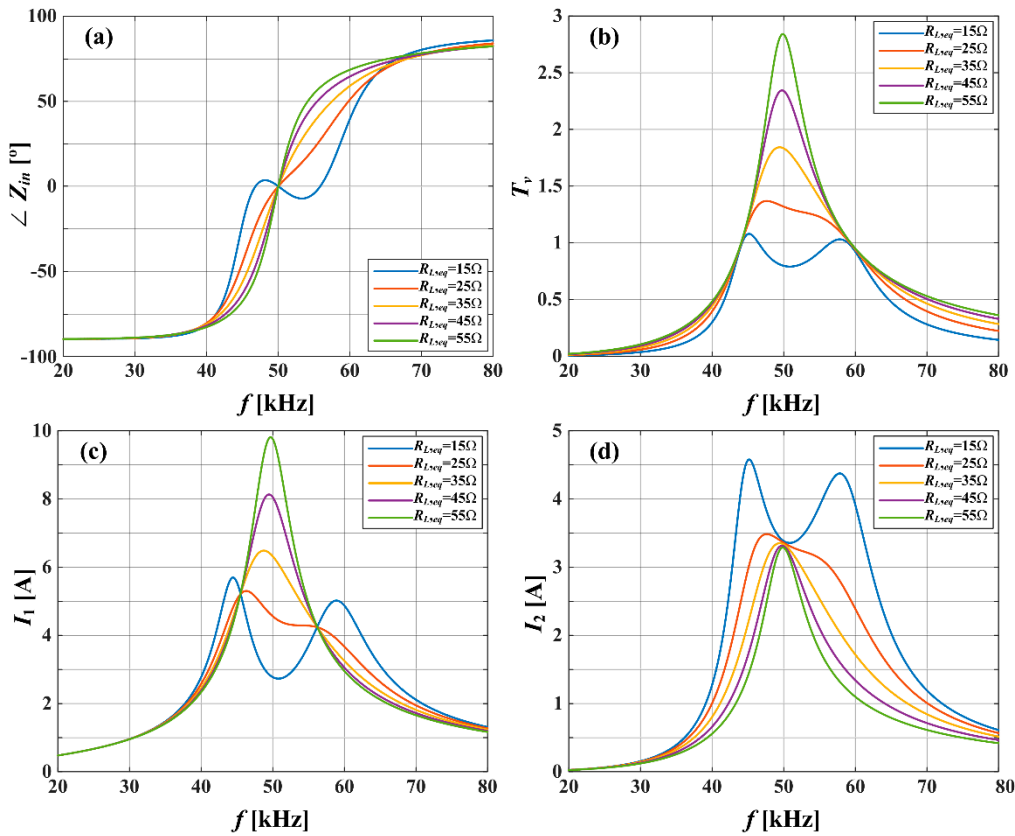


Figure 4. Electrical characteristics of the S-S WPT circuit for $V_{DC} = 50$ V, $\phi = 0$, $L_1 = 202.49$ μ H, $L_2 = 202.06$ μ H, $C_1 = 49.97$ nF, $C_2 = 50.09$ nF, $M_{12} = 59.18$ μ H, $R_{in} = 12$ m Ω , $R_1 = 252$ m Ω , and $R_2 = 248$ m Ω : (a) phase angle of Z_{in} ; (b) voltage gain T_v ; (c) amplitude of I_1 ; and (d) amplitude of I_2 .

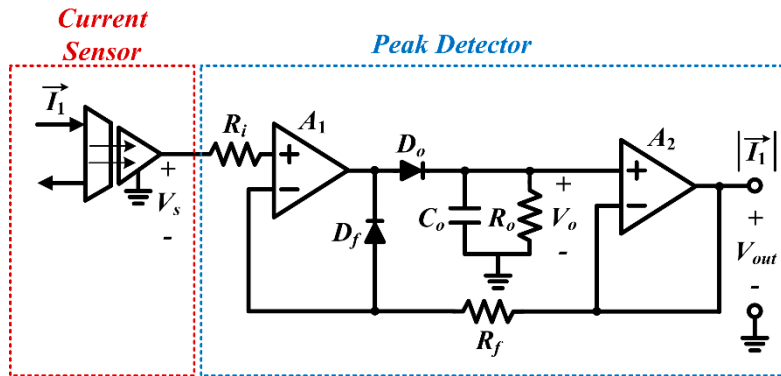


Figure 5. The peak detection circuit to measure the peak current of the transmitter coil.

To estimate the load conditions, the peak detection circuit measures the peak current $I_{1,o}$ at $f = f_o$ and $I_{1,a}$ at $f = f_a$, respectively, and uses simple mathematical equations for the input impedance. The measurement time of $I_{1,o}$ and $I_{1,a}$ is short, so the load conditions are assumed to remain constant during the estimation process. Also, the system parameters of the transmitter side (V_{DC} , ϕ , L_1 , C_1 and R_1) and receiver side (L_2 , C_2 and R_2) are assumed to be known, and the proposed method predicts M_{12} , $R_{L,eq}$, I_{bat} , and V_{bat} .

At first, the circuit operates at $f = f_o$, and the M_{12} can be expressed using detected $I_{1,o}$ and Equation (8) as

$$M_{12}^2 = \frac{[R_2 + R_{L,eq}] \cdot [V_{1,o} - I_{1,o}(R_{in} + R_1)]}{\omega_o^2 \cdot I_{1,o}} \quad (12)$$

where $V_{1,o}$ is the peak voltage of the transmitter coil at $f = f_o$, $V_{1,o} = 2V_{DC}(1 + \cos \phi)/\pi$ from Equation (1), and the unknown parameters of Equation (12) are M_{12} and $R_{L,eq}$.

Then, the circuit operates at $f = f_a$, and the square of the absolute value of input impedance $\left| \vec{Z}_{in,a} \right|^2 = V_{1,a}^2 / I_{1,a}^2$ can be expressed using Equation (8) as

$$\left| \vec{Z}_{in,a} \right|^2 = (R_1 + R_{in})^2 + (\omega_a L_1 - 1/\omega_a C_1)^2 + \frac{2\omega_a^2 M_{12}^2 \{ (R_1 + R_{in})(R_2 + R_{L,eq}) - (\omega_a L_1 - 1/\omega_a C_1)(\omega_a L_2 - 1/\omega_a C_2) \} + \omega_a^4 M_{12}^4}{(R_2 + R_{L,eq})^2 + (\omega_a L_2 - 1/\omega_a C_2)^2}, \quad (13)$$

where $V_{1,a}$, $I_{1,a}$ is the peak voltage and current of transmitter coil at $f = f_a$, $V_{1,a} = 2V_{DC}(1 + \cos \phi)/\pi$ from Equation (1). In this equation, the unknown parameters are the same as Equation (12).

If Equation (12) is applied to Equation (13), the $R_{L,eq}$ can be arranged as $\alpha R_{L,eq}^2 + \beta R_{L,eq} + \gamma = 0$, where α , β and γ are as follows:

$$\alpha = \omega_o^4 I_{1,o}^2 \left| \vec{Z}_{in,a} \right|^2 - \omega_o^4 I_{1,o}^2 \{ (R_1 + R_{in})^2 + (\omega_a L_1 - 1/\omega_a C_1)^2 \} - 2\omega_a^2 \omega_o^2 I_{1,o} \{ R_1 + R_{in} \} \cdot \{ V_{1,o} - I_{1,o}(R_{in} + R_1) \} - \omega_a^4 \{ V_{1,o} - I_{1,o}(R_{in} + R_1) \}^2 \quad (14)$$

$$\beta = 2R_2 \omega_o^4 I_{1,o}^2 \left| \vec{Z}_{in,a} \right|^2 - 2R_2 \omega_o^4 I_{1,o}^2 \{ (R_1 + R_{in})^2 + (\omega_a L_1 - 1/\omega_a C_1)^2 \} - 2\omega_a^2 \omega_o^2 I_{1,o} \{ 2R_2(R_1 + R_{in}) - (\omega_a L_1 - 1/\omega_a C_1)(\omega_a L_2 - 1/\omega_a C_2) \} \cdot \{ V_{1,o} - I_{1,o}(R_{in} + R_1) \} - 2R_2 \omega_a^4 \{ V_{1,o} - I_{1,o}(R_{in} + R_1) \}^2 \quad (15)$$

$$\gamma = \omega_o^4 I_{1,o}^2 \left| \vec{Z}_{in,a} \right|^2 \{ R_2^2 + (\omega_a L_2 - 1/\omega_a C_2)^2 \} - \omega_o^4 I_{1,o}^2 \{ (R_1 + R_{in})^2 + (\omega_a L_1 - 1/\omega_a C_1)^2 \} \cdot \{ R_2^2 + (\omega_a L_2 - 1/\omega_a C_2)^2 \} - \omega_a^4 R_2^2 \{ V_{1,o} - I_{1,o}(R_{in} + R_1) \}^2 - 2\omega_a^2 \omega_o^2 I_{1,o} \{ R_2^2(R_1 + R_{in}) - R_2(\omega_a L_1 - 1/\omega_a C_1)(\omega_a L_2 - 1/\omega_a C_2) \} \cdot \{ V_{1,o} - I_{1,o}(R_{in} + R_1) \} \quad (16)$$

This equation has two solutions for $R_{L,eq}$, and the smaller one is a reasonable value according to the calculation result, so estimated load resistance $R_{L,eq,est}$ and estimated equivalent resistance of battery $R_{bat,est}$ can be estimated as

$$R_{L,eq,est} = \frac{-\beta - \sqrt{\beta^2 - 4\alpha \cdot \gamma}}{2\alpha} = \frac{8}{\pi^2} \cdot R_{bat,est}. \quad (17)$$

Then, the estimated mutual inductance $M_{12,est}$ can also be derived by applying Equation (17) to Equation (12) as:

$$M_{12,est} = \sqrt{\frac{[2\alpha \cdot R_2 - \beta - \sqrt{\beta^2 - 4\alpha \cdot \gamma}] \cdot [V_{1,o} - I_{1,o}(R_{in} + R_1)]}{2\alpha \cdot \omega_o^2 \cdot I_{1,o}}}. \quad (18)$$

Other important estimated load parameters $I_{bat,est}$ and $V_{bat,est}$ at $f = f_o$ can be expressed using Equations (1)–(7), (17), and (18) as

$$I_{bat,est} = \frac{2I_{1,o}}{\pi} \cdot \frac{\omega_o M_{12,est}}{R_2 + R_{L,eq,est}} \quad (19)$$

$$V_{bat,est} = \frac{\pi^2}{8} \cdot I_{bat,est} \cdot R_{L,eq,est}. \quad (20)$$

Finally, the proposed method can predict $R_{L,eq}$, M_{12} , I_{bat} , and V_{bat} , and does not need a high sampling frequency to measure AC voltage and current, similar to previous studies [14–19].

2.3. Control Method of the S-S WPT Circuit for Battery Charging

The battery should be charged in CC mode when $V_{bat} \leq V_{bat,cut}$, and in CV mode when $V_{bat} > V_{bat,cut}$. In CV mode, I_{bat} decreases as V_{bat} increases, until I_{bat} reaches the end charging current I_{end} at which the charging operation stops [9–12].

T_v and I_2 in Equations (9) and (11) depend on $R_{L,eq}$, which varies as the charge state of battery varies. When all ESRs are negligibly small, Equation (11) gives I_2 at $\omega = \omega_o$ as

$$I_2 = \frac{\omega_o M_{12} V_1}{(R_{in} + R_1)(R_2 + R_{L,eq}) + \omega_o^2 M_{12}^2} \approx \frac{V_1}{\omega_o M_{12}}, \quad (21)$$

because $Z_1 = R_1$ and $Z_2 = R_2$ when $\omega = \omega_o$. This equation indicates that the WPT circuit can be operated in CC mode if all ESRs are ignored and $\omega = \omega_o$. However, ESRs affect the capability of CC regulation (Figure 4d), so a separate control method should be introduced to attain CC mode; the proposed WPT circuit applies phase shift control of the full-bridge inverter at $f = f_o$, and the ϕ to maintain the CC output is compensated by using the proportional integral (PI) controller, which can be calculated as

$$\phi = \cos^{-1} \left\{ \frac{\pi^2 \cdot (I_{ref}/2) \cdot [(R_{in} + R_1)(R_2 + R_{L,eq,est}) + \omega_o^2 M_{12,est}^2]}{2\omega_o M_{12,est} V_{DC}} - 1 \right\}, \quad (22)$$

where I_{ref} is the predetermined charging current reference. If ESRs are very small in CC mode, the influence of $R_{L,eq}$ in ϕ will also be very small.

To operate the WPT circuit in CV mode, T_v should not depend on $R_{L,eq}$. If all ESRs are negligible, Equation (9) can be approximated as

$$T_v \approx \left| [j\omega M_{12}] / [(j\omega L_1 + 1/j\omega C_1) + \kappa/R_{L,eq}] \right|, \quad (23)$$

where $\kappa = \omega^2(M_{12}^2 - L_1 L_2) - 1/(\omega^2 C_1 C_2) + L_1/C_2 + L_2/C_1$. After setting $\kappa = 0$, the frequencies f_{CV1} and f_{CV2} for CV operation are obtained as $f_{CV1} = 2\pi \cdot f_o / \sqrt{1 + k_{12}}$ and $f_{CV2} = 2\pi \cdot f_o / \sqrt{1 - k_{12}}$, and T_v at $f = f_{CV1}$ or $f = f_{CV2}$ is calculated using Equation (23) and $M_{12} = k_{12} \sqrt{L_1 L_2}$ as $T_v = \sqrt{L_2/L_1}$. However, ESRs in CV mode are also difficult to ignore, and if f_{CV1} and f_{CV2} deviate too much from f_o , the system efficiency also drastically decreases [14]. Therefore, the proposed WPT circuit still operates at $f = f_o$ in CV mode, and the ϕ to maintain the CV output is compensated by using the PI controller, which can be calculated as

$$\phi = \cos^{-1} \left\{ \frac{4CVL \cdot [(R_{in} + R_1)(R_2 + R_{L,eq,est}) + \omega_o^2 M_{12,est}^2]}{2\omega_o M_{12,est} V_{DC} R_{L,eq,est}} - 1 \right\}. \quad (24)$$

The influence of $R_{L,eq}$ in CV mode cannot be ignored, even if ESRs are very small. Thus, ϕ will increase as $R_{L,eq}$ increases.

Finally, the proposed S-S WPT circuit applies the control algorithm (Figure 6) for battery charging, and it consists of the following procedures:

- (1) Modulate the WPT circuit at $f = f_o$ and f_a ; sense the $I_{1,o}$ and $I_{1,a}$, respectively.
- (2) Using the $I_{1,o}$ and $I_{1,a}$, estimate $R_{bat,est}[1] = V_{bat,est}[1] / I_{bat,est}[1]$ and $M_{12,est}$.
- (3) If $V_{bat,est}[1] < CVL$, begin the control procedure. Otherwise, turn off the S-S WPT circuit.
- (4) Set $f = f_o$ to operate the WPT circuit in the CC mode.
- (5) Using the PI controller, adjust $\phi[n]$ such that $I_{bat,est}$ equals to I_{ref} .
- (6) Estimate the $R_{bat,est}[n] = V_{bat,est}[n] / I_{bat,est}[n]$ by using $I_{1,o}[n]$ and (12); $R_{bat,est}[n]$ is continuously updated to follow the charging profile of battery.
- (7) Repeat (5)–(6) until $V_{bat,est}[n] = CVL$.
- (8) Change the operation of WPT circuit from the CC to CV mode, and maintain $f = f_o$.
- (9) Using the PI controller, adjust $\phi[n]$ such that $V_{bat,est} = CVL$.
- (10) Repeat procedure 6 until $I_{bat,est}[n] = I_{end}$.
- (11) Turn off the S-S WPT circuit.

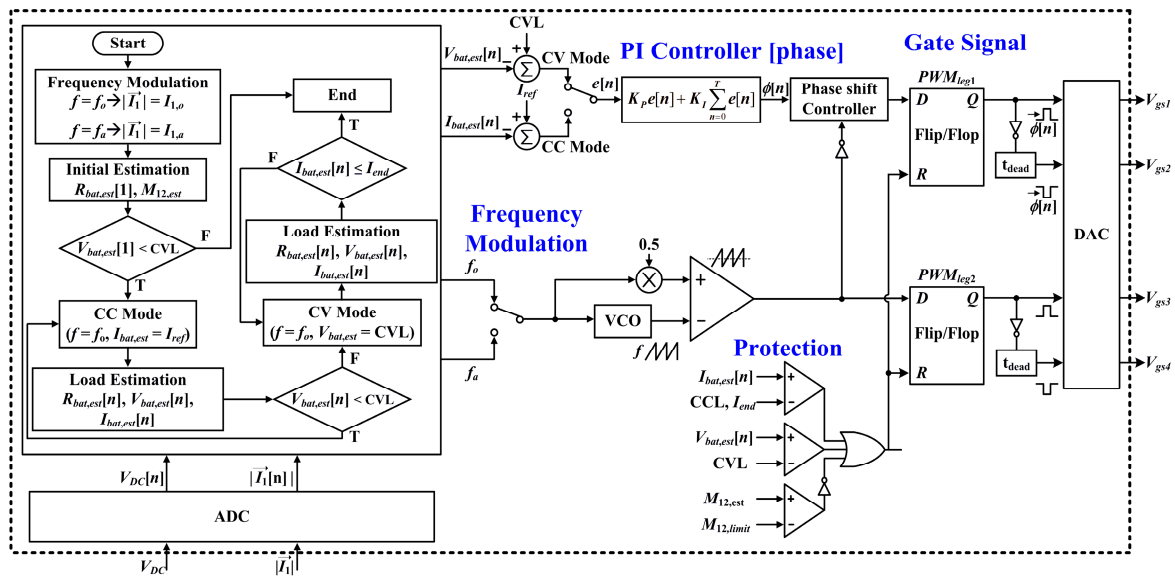


Figure 6. A block diagram of the digital controller for the S-S wireless battery charging circuit.

The controller has a protection function for charging current limit (CCL), CVL, and coil alignment of the WPT circuit. When $M_{12,est} < M_{12,limit}$, the controller terminates the battery-charging operation, because the alignment of the coils is inappropriate for battery charging.

3. Experimental Results

The experimental S-S WPT circuit for battery charging (Figure 7a,b) was built and tested to prove the proposed control method. Two identical coils had an inner diameter of 100 mm and outer diameter of 200 mm; $L_1 = 202.49 \mu\text{H}$, $L_2 = 202.06 \mu\text{H}$, and $C_1 = C_2 = 50 \text{ nF}$ were chosen for $f_0 = 50 \text{ kHz}$. The input voltage V_{DC} was 50 V, and the sampling frequency to sense the output value of the peak detector was set as 50 kHz, which was simply synchronized to the f_0 . The values of circuit parameters are given in Table 1.

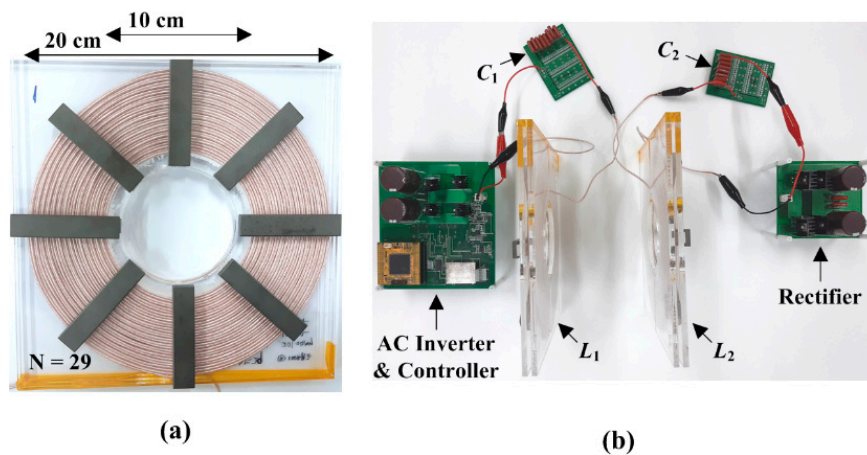


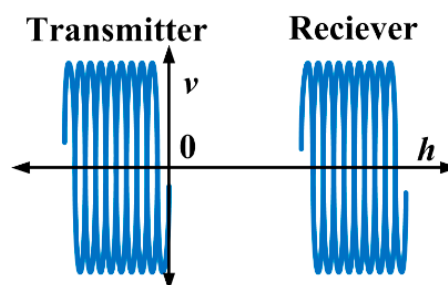
Figure 7. Photograph of the (a) transmitter coil and (b) experimental S-S WPT circuit.

Table 1. Circuit parameters for the experimental circuit.

| Component | Value (Model) |
|---------------|----------------------|
| L_1 | 202.49 μH |
| L_2 | 202.06 μH |
| C_1 | 49.97 nF |
| C_2 | 50.09 nF |
| R_{in} | 12 m Ω |
| R_1 | 252 m Ω |
| R_2 | 248 m Ω |
| Q_1 – Q_4 | FDP0715N15A |
| D_1 – D_4 | 30ETH06 |
| Controller | TMS320F28335 |

First, the load estimation was performed using the method in Section 2.2. R_{bat} and M_{12} between the transmitter and receiver coils were measured and estimated using electrical load (DL1000H; NF, Co., Ltd.) and a inductance, capacitance and resistance (LCR) meter. The coil alignment was modulated on either the separation h in the axial direction of the coil or the misalignment v in the radial direction (Figure 8). At $h = 6$ cm and $v = 0$ cm, the WPT circuit was operated at $f_o = 50$ kHz and $f_a = 55$ kHz to estimate the load condition, and $R_{bat} = 20.11 \Omega$ and $M_{12} = 48.81 \mu\text{H}$ at $\phi = 0$. The measured $I_{1,o} = 4.21$ A (Figure 9a) and $I_{1,a} = 5.08$ A (Figure 9b), and the estimated load conditions were $R_{bat,est} = 20.49 \Omega$ and $M_{12,est} = 49.30 \mu\text{H}$ by using Equations (17) and (18). The errors of estimation results were -1.88% and -1.86% , respectively; other estimation results were obtained while varying h , v , and R_{bat} (Tables 2 and 3). Here, h was varied in the range of 5–7 cm at $v = 0$ cm, v was varied in the range of 0–6 cm at $h = 0$ cm, and R_{bat} was varied in the range of 15.06–25.17 Ω . As a result, the proposed method estimated the R_{bat} and M_{12} within absolute errors at $<3.87\%$ and $<3.38\%$, respectively. These experimental results demonstrate the usefulness of the proposed load estimation method. The errors of estimation were caused by inductance variation according to the coil alignment conditions and measurement error at f_o and f_a . A detailed error analysis is given in the next section.

The current and voltage regulation for the battery charging were implemented using the controller proposed in Section 2.3. An electrical load was used to emulate the battery pack, which was assumed to have $30 \text{ V} \leq V_{bat} \leq 48 \text{ V}$ (corresponding to a pack of 12 serially connected Li-ion battery cells). The R_{bat} of the battery pack was $15 \Omega \leq R_{bat} \leq 24 \Omega$ for CC charging at $I_{ref} = 2$ A and $24 \Omega \leq R_{bat} \leq 240 \Omega$ for CV charging at $CVL = 48$ V and $I_{end} = 200$ mA. The transmitter and receiver coils were located at $h = 5$ cm and $v = 0$ cm. In procedures 1 and 2, the controller of the WPT circuit used $f_o = 50$ kHz and $f_a = 55$ kHz; $R_{bat,est}(1) = 15.51 \Omega$ at $R_{bat} = 15.01 \Omega$ (-3.33% error) and $M_{12,est} = 59.78 \mu\text{H}$ at $M_{12} = 59.18 \mu\text{H}$ (-1.01% error). Because $V_{bat,est}(1) = 31.02 \text{ V} < CVL$ in procedure 3, the controller began the charging control procedures in steps 4–11.

**Figure 8.** Alignment schematic of the two coils from top view.

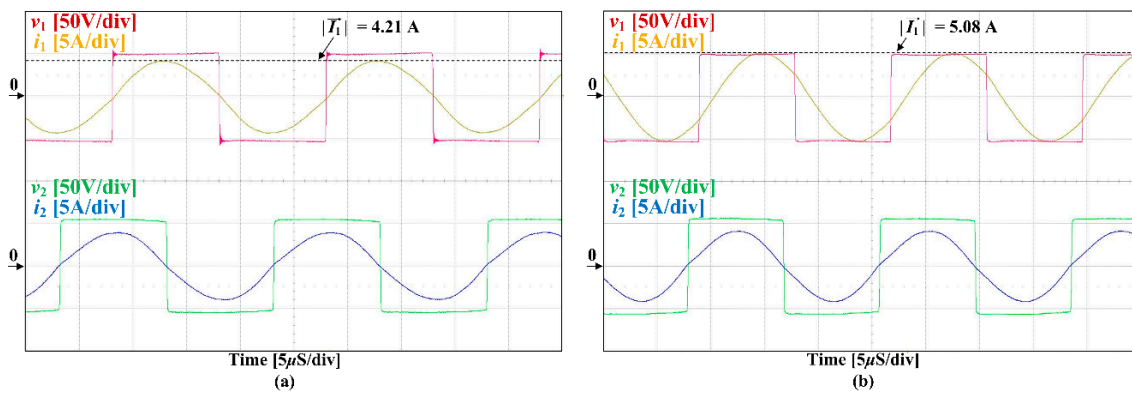


Figure 9. Operation wave forms of the proposed WPT circuit: (a) v_1 , i_1 , v_2 , and i_2 at $f_o = 50$ kHz; (b) v_1 , i_1 , v_2 , and i_2 at $f_o = 55$ kHz.

Table 2. Estimation results for R_{bat} .

| h, v (cm) | R_{bat} (Ω) | $R_{bat,est}$ (Ω) (Error (%)) | R_{bat} (Ω) | $R_{bat,est}$ (Ω) (Error (%)) | R_{bat} (Ω) | $R_{bat,est}$ (Ω) (Error (%)) |
|-------------|------------------------|---|------------------------|---|------------------------|---|
| 5, 0 | | 15.20 (−0.92) | | 19.61 (2.48) | | 24.22 (3.77) |
| 6, 0 | | 15.60 (−3.58) | | 20.49 (−3.58) | | 25.31 (−0.55) |
| 7, 0 | | 15.54 (−3.18) | | 20.54 (−2.08) | | 25.35 (−0.71) |
| 5, 2 | 15.06 | 15.46 (−2.66) | 20.11 | 19.72 (1.90) | 25.17 | 24.19 (3.87) |
| 5, 4 | | 15.45 (−2.58) | | 20.37 (−1.29) | | 25.11 (0.23) |
| 5, 6 | | 15.60 (−3.58) | | 20.27 (−0.79) | | 24.84 (1.31) |

Table 3. Estimation results for M_{12} .

| h, v (cm) | M_{12} (μH) | $M_{12,est}$ (μH) @ 15.06 Ω (Error (%)) | $M_{12,est}$ (μH) @ 20.11 Ω (Error (%)) | $M_{12,est}$ (μH) @ 25.17 Ω (Error (%)) |
|-------------|----------------------------|---|---|---|
| 5, 0 | 59.18 | 58.41 (1.30) | 58.7 (0.81) | 59.03 (0.26) |
| 6, 0 | 48.81 | 49.27 (−0.92) | 49.73 (−1.86) | 49.76 (−1.92) |
| 7, 0 | 40.76 | 41.12 (−3.18) | 41.59 (−2.08) | 41.62 (−2.08) |
| 5, 2 | 57.28 | 55.37 (3.38) | 55.73 (2.71) | 55.85 (2.50) |
| 5, 4 | 49.54 | 49.28 (0.53) | 49.68 (−0.26) | 49.79 (−0.49) |
| 5, 6 | 38.66 | 39.55 (−2.28) | 39.49 (−2.12) | 39.44 (−1.99) |

In the CC mode of procedures 4–7, the waveform (Figure 10) shows that v_1 and i_1 had the same phase because the S-S WPT circuit operated at $f = f_o$, and that ϕ was compensated to regulate $I_{bat,est} = I_{ref}$. When the circuit operated at $R_{bat} = 15.01 \Omega$ (Figure 10a), $I_{bat} = 2.07$ A (−3.5% error) and $V_{bat} = 31.21$ V. In this CC mode, V_{bat} increased as R_{bat} increased because $I_{bat,est}$ tracked the predetermined $I_{ref} = 2$ A. The waveform of Figure 10b shows that V_{bat} increased to 46.55 V at $R_{bat} = 22.47 \Omega$, while $I_{bat} = 2.07$ A (−3.5% error). When procedure 5 was used in the CC mode, the range of regulated I_{bat} was 2.074–2.079 A; the tracking absolute error was <3.95% (Figure 12). The power transfer efficiency of the CC mode gradually increased as R_{bat} increased, and the range of it was 88.81–92.05% (Figure 13). After $V_{bat,est}$ reached CVL = 48 V, the charging mode was changed to CV mode in the procedures 8–11.

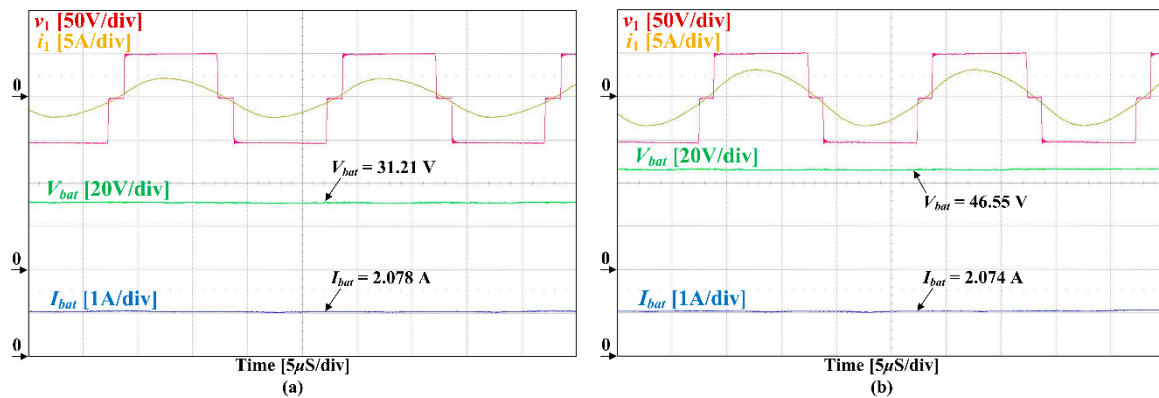


Figure 10. Operation wave forms of the proposed WPT circuit: v_1 , i_1 , V_{bat} , and I_{bat} in the CC mode (a) at $R_{bat} = 15.01 \Omega$ and (b) at $R_{bat} = 22.47 \Omega$.

The waveform of CV mode (Figure 11) also shows that v_1 and i_1 had the same phase because the S-S WPT circuit operated at $f = f_o$, and that ϕ was compensated to regulate $V_{bat,est} = CVL$. When the circuit operated at $R_{bat} = 54.10 \Omega$ (Figure 11a), $V_{bat} = 47.24 \text{ V}$ (1.58% error) and $I_{bat} = 0.88 \text{ A}$. In this CV mode, as R_{bat} increased, T_v increased (Figure 4b); ϕ should be increased to maintain V_{bat} . Thus, I_{bat} gradually decreased until $I_{bat,est} = I_{end}$. The waveform of Figure 11b shows that I_{bat} decreased to 0.2 A at $R_{bat} = 244 \Omega$, while $V_{bat} = 47.92 \text{ V}$ (0.16% error). When procedure 9 was used, the range of regulated V_{bat} was $47.09\text{--}47.92 \text{ V}$; the tracking absolute error was $<1.89\%$ (Figure 12). The power transfer efficiency of the CV mode gradually decreased as R_{bat} increased, and the range was $74.77\text{--}92.49\%$ (Figure 13).

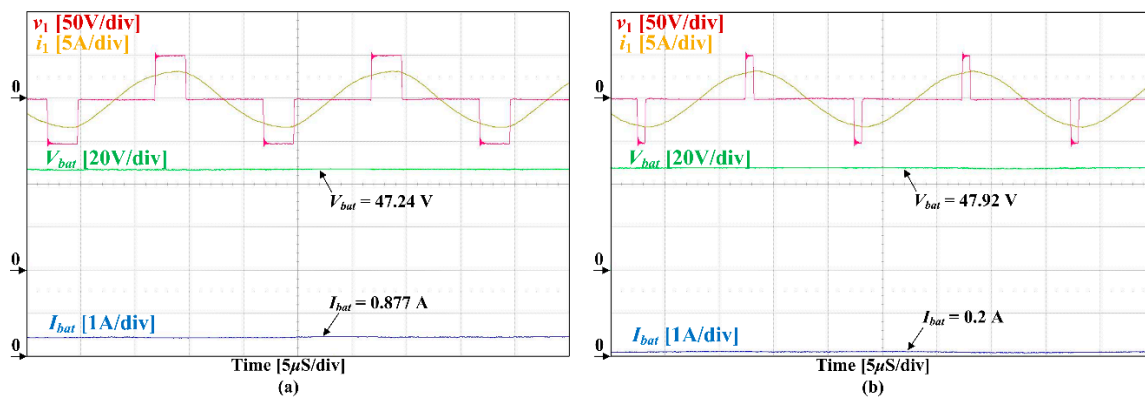


Figure 11. Operation wave forms of the proposed WPT circuit: v_1 , i_1 , V_{bat} , and I_{bat} in the CV mode (a) at $R_{bat} = 54.10 \Omega$ and (b) at $R_{bat} = 244 \Omega$.

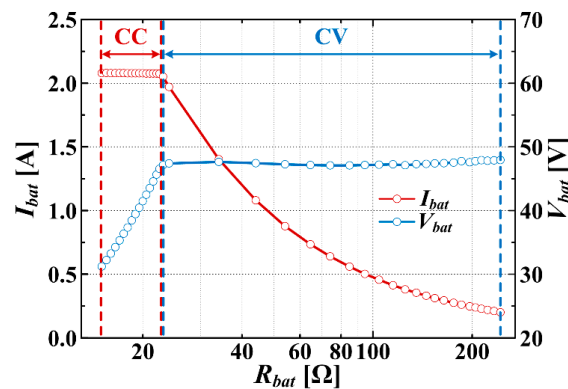


Figure 12. Measurement of regulated I_{bat} and V_{bat} in constant current (CC) and constant voltage (CV) modes.

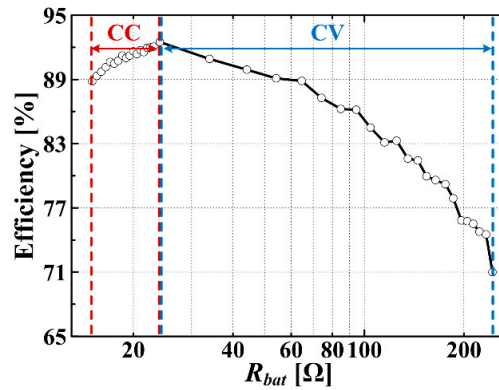


Figure 13. Power transfer efficiency of the proposed WPT circuit in CC and CV modes.

These results show that the proposed load estimation method is suitable for use in battery charging, and that the adjustment of ϕ was crucial to have I_{bat} follow I_{ref} in CC charging mode and to have V_{bat} follow CVL in CV charging mode.

4. Error Analysis

In the proposed estimation method, the errors of estimation results can be generated using the deviated inductance (L_{dev}) according to the coil alignment and measurement error of input impedance at f_o and f_a . Therefore, these errors of the proposed method were analyzed by using MATLAB (R2015a, MathWorks, Massachusetts, USA) in this section.

In this section, the errors of estimation results due to the L_{dev} (Figure 14a,b) were calculated as

$$\text{Error}(R_{bat,est,dev}) = [(R_{bat} - R_{bat,est}(L_{dev})) / R_{bat}] \times 100, \quad (25)$$

$$\text{Error}(M_{12,est,dev}) = [(M_{12} - M_{12,est}(L_{dev})) / M_{12}] \times 100, \quad (26)$$

where $R_{bat,est}(L_{dev})$ and $M_{12,est}(L_{dev})$ are estimated R_{bat} and M_{12} in the L_{dev} . The measurement errors of input impedance (Figure 14c–f) were calculated as

$$\text{Error}|\vec{Z}_{in,a}| = [(|\vec{Z}_{in,a}| - |\vec{Z}_{in,a,measure}|) / |\vec{Z}_{in,a}|] \times 100, \quad (27)$$

$$\text{Error}|\vec{Z}_{in,o}| = [(|\vec{Z}_{in,o}| - |\vec{Z}_{in,o,measure}|) / |\vec{Z}_{in,o}|] \times 100, \quad (28)$$

where $|\vec{Z}_{in,a,measure}|$ and $|\vec{Z}_{in,o,measure}|$ are measured values of $|\vec{Z}_{in,a}|$ and $|\vec{Z}_{in,o}|$ at $f = f_a$ and $f = f_o$ by using a peak detection circuit in Figure 5. Then, the errors of estimation results due to the $\text{Error}|\vec{Z}_{in,a}|$ and $\text{Error}|\vec{Z}_{in,o}|$ (Figure 14c–f) were calculated as

$$\text{Error}(R_{bat,est,fa}) = [(R_{bat} - R_{bat,est}(|\vec{Z}_{in,a,measure}|)) / R_{bat}] \times 100, \quad (29)$$

$$\text{Error}(M_{12,est,fa}) = [(M_{12} - M_{12,est}(|\vec{Z}_{in,a,measure}|)) / M_{12}] \times 100, \quad (30)$$

$$\text{Error}(R_{bat,est,fo}) = [(R_{bat} - R_{bat,est}(|\vec{Z}_{in,o,measure}|)) / R_{bat}] \times 100, \quad (31)$$

$$\text{Error}(M_{12,est,fo}) = [(M_{12} - M_{12,est}(|\vec{Z}_{in,o,measure}|)) / M_{12}] \times 100, \quad (32)$$

where $R_{bat,est}(\vec{Z}_{in,a,measure})$ and $M_{12,est}(\vec{Z}_{in,a,measure})$ are $R_{bat,est}$ and $M_{12,est}$ in the Error $|\vec{Z}_{in,a}|$, and $R_{bat,est}(\vec{Z}_{in,o,measure})$ and $M_{12,est}(\vec{Z}_{in,o,measure})$ are $R_{bat,est}$ and $M_{12,est}$ in the Error $|\vec{Z}_{in,o}|$.

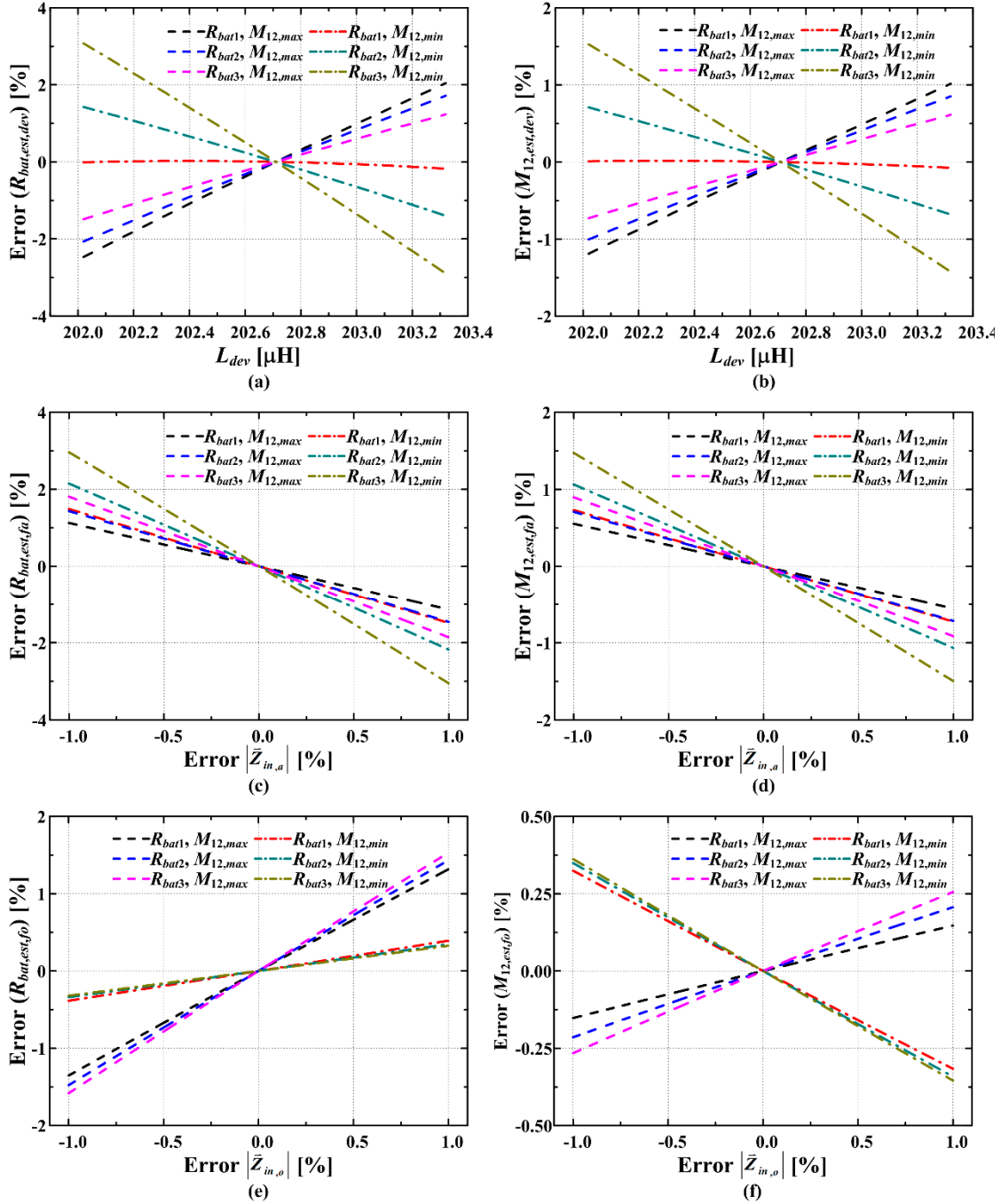


Figure 14. Error analyses (a) of $R_{bat,est}$ with inductance deviation, (b) of $M_{12,est}$ with inductance deviation, (c) of $R_{bat,est}$ with measurement error at f_a , (d) of $M_{12,est}$ with measurement error at f_a , (e) of $R_{bat,est}$ with measurement error at f_o , and (f) of $M_{12,est}$ with measurement error at f_o .

At first, the coil alignment of the proposed estimation method was verified in the range of $h = 5\text{--}7$ cm at $v = 0$ cm and $v = 0\text{--}6$ cm at $v = 5$ cm. In this misalignment range of coils, the self-inductance of L_1 and L_2 was changed according to the effect of the magnetic field between coils. The variation range of $L_1 = 202.01\text{--}203.41$ μH , and $L_2 = 201.50\text{--}202.94$ μH in $M_{12} = 38.66\text{--}59.18$ μH . In this error analysis,

according to the L_{dev} , the simulation parameters were set as $L_1 = L_2 = 202.71 \mu\text{H}$, $C_1 = C_2 = 49.97 \text{ nF}$, $R_{in} = 12 \text{ m}\Omega$, $R_1 = 252 \text{ m}\Omega$, and $R_2 = 248 \text{ m}\Omega$. Then, the L_{dev} was equivalently set between L_1 and L_2 as $L_{dev} = L_{1,dev} = L_{2,dev} = 202.02\text{--}203.41 \mu\text{H}$, $R_{bat1} = 15 \Omega$, $R_{bat2} = 20 \Omega$, $R_{bat3} = 25 \Omega$, $M_{12,max} = 59.18 \mu\text{H}$, and $M_{12,min} = 38.66 \mu\text{H}$. The $\text{Error}\left|\vec{Z}_{in,a}\right|$ and $\text{Error}\left|\vec{Z}_{in,o}\right|$ were set to zero in this analysis, and only L_{dev} was considered. As a result, the $\text{Error}(R_{bat,est,dev})$ and $\text{Error}(M_{12,est,dev})$ increased as R_{bat} decreased at $M_{12,max}$ and R_{bat} increased at $M_{12,min}$ (Figure 14a,b). Also, the $\text{Error}(R_{bat,est,dev})$ and $\text{Error}(M_{12,est,dev})$ due to the variation of R_{bat} ($R_{bat1}\text{--}R_{bat3}$) were more sensitive at $M_{12,min}$ than $M_{12,max}$.

Secondly, the proposed estimation method measures the $\left|\vec{Z}_{in,a,measure}\right|$ and $\left|\vec{Z}_{in,o,measure}\right|$, and the $\text{Error}\left|\vec{Z}_{in,a}\right|$ and $\text{Error}\left|\vec{Z}_{in,o}\right|$ have an effect on the accuracy of the estimation. In this error analysis, according to the $\text{Error}\left|\vec{Z}_{in,a}\right|$ and $\text{Error}\left|\vec{Z}_{in,o}\right|$, $\text{Error}(R_{bat,est,fa})$, $\text{Error}(M_{12,est,fa})$, $\text{Error}(R_{bat,est,fo})$, and $\text{Error}(M_{12,est,fo})$ were analyzed under the $\pm 1\%$ variation of $\text{Error}\left|\vec{Z}_{in,a}\right|$ and $\text{Error}\left|\vec{Z}_{in,o}\right|$, and the simulation parameters were equivalently set as the error analysis of Equations (25) and (26). The $\text{Error}(R_{bat,est,dev})$ and $\text{Error}(M_{12,est,dev})$ were set to zero in this analysis. In the $\text{Error}\left|\vec{Z}_{in,a}\right|$, the $\text{Error}(R_{bat,est,fa})$ and $\text{Error}(M_{12,est,fa})$ increased as R_{bat} increased, and were larger at $M_{12,min}$ than $M_{12,max}$ in the same R_{bat} (Figure 14c,d). In the $\text{Error}\left|\vec{Z}_{in,o}\right|$ at $M_{12,max}$, the $\text{Error}(R_{bat,est,fo})$ and $\text{Error}(M_{12,est,fo})$ increased as R_{bat} increased. At $M_{12,min}$, the $\text{Error}(R_{bat,est,fo})$ increased as R_{bat} decreased, and $\text{Error}(M_{12,est,fo})$ increased as R_{bat} increased (Figure 14e,f). Overall, the $\text{Error}\left|\vec{Z}_{in,a}\right|$ had more impact on the accuracy of proposed estimation method than the $\text{Error}\left|\vec{Z}_{in,o}\right|$.

In conclusion, the errors of estimation results were $<3\%$ in Equations (25), (29), and (31), and $<1.5\%$ in Equations (26), (30) and (32). Also, Equations (25) and (26) (Figure 14a,b) were more sensitive to the variation of R_{bat} and M_{12} than Equations (29)–(32) (Figure 14c–f). In the practical applications, the proposed controller (Figure 6) includes the protection function to limit the range of coil alignment as $M_{12,est} < M_{12,limit}$, and the auxiliary positioning device can be introduced to minimize the inductance deviation.

5. Conclusions

This paper presents a wireless battery charging circuit that uses a new load estimation method. The proposed method estimates R_L , M_{12} , V_{bat} , and I_{bat} without any wireless communication by using a simple peak detection circuit to sense the peak current of the transmitter coil; it samples this peak current as a DC value. After the peak current values are sampled at resonant frequency f_0 and auxiliary frequency f_a , the estimation is performed by using the magnitude of the input impedance. Thus, this method does not need a high sampling frequency to detect the AC voltage and the current of the transmitter coil. When the proposed WPT circuit is operated to charge a battery pack, the circuit uses the proposed load estimation method and phase ϕ control of the full-bridge inverter to regulate the output current and voltage. A prototype circuit to charge a 48-V battery pack was tested under the various load resistance and coil alignment conditions. Then, the errors of estimation results due to the inductance variation and measurement error were analyzed. Finally, all experimental and simulation results indicated that the proposed method is well suited to control the WPT battery charging circuit efficiently.

Author Contributions: S.-W.L. developed the circuit and load estimation method, constructed the hardware prototype, and conducted the experiments. Y.-G.C. and J.-H.K. supported the experiments and analyzed the experimental results. B.K. provided guidance and key suggestions for this study.

Funding: This research was supported by the MSIT (Ministry of Science and ICT), Korea, under the “ICT Consilience Creative program” (IITP-2019-2011-1-00783) supervised by the IITP (Institute for Information & communications Technology Promotion).

Conflicts of Interest: The authors declare no conflict of interest.

Nomenclature

| | |
|--|--|
| Q_1-Q_4 | Switches of full bridge inverter. |
| D_1-D_4 | Diodes of full bridge rectifier. |
| L_1, L_2 | Transmitter and receiver coil (H). |
| C_1, C_2 | Resonant capacitors of transmitter and receiver coil (F). |
| ω, f | Angular switching frequency and switching frequency (rad/s), (Hz). |
| ω_0, f_0 | Resonance angular frequency and resonance frequency (rad/s), (Hz). |
| f_a | auxiliary switching frequency (Hz). |
| V_{DC} | DC input voltage of full-bridge inverter (V). |
| $V_{bat}, V_{bat,cut}$ | Output voltage (battery voltage) and predetermined limit voltage of battery (V). |
| I_{bat} | Output current (battery charging current) (A). |
| η_e | Power transfer efficiency (%). |
| k_{12}, M_{12} | Coupling coefficient and mutual inductance (H). |
| $M_{12,limit}$ | Limitation of M_{12} in charging controller for proposed circuit (H). |
| f_{cc}, f_{cv} | Switching frequency for constant current and voltage (Hz). |
| R_L | Load resistance (Ω). |
| $v_1(t), i_1(t)$ | Voltage and current of transmitter coil (V), (A). |
| \vec{V}_1, \vec{I}_1 | Voltage and current vector of transmitter coil. |
| V_1, I_1 | Amplitude of \vec{V}_1 and \vec{I}_1 (V), (A). |
| $v_2(t), i_2(t)$ | Voltage and current of receiver coil (V), (A). |
| \vec{V}_2, \vec{I}_2 | Voltage and current vector of receiver coil. |
| V_2, I_2 | Amplitude of $v_2(t)$ and $i_2(t)$ (V), (A). |
| ϕ | Switching phase difference between lags of full-bridge inverter (rad). |
| θ | Phase difference between $v_1(t)$ and $i_1(t)$ (rad). |
| ϕ | Phase difference between $i_1(t)$ and $v_2(t), i_2(t)$ (rad). |
| R_{in}, R_1, R_2 | Equivalent series resistance of full-bridge inverter, primary and secondary coil (Ω). |
| $R_{bat}, R_{L,eq}$ | Resistance of battery and equivalent resistance of R_{bat} (Ω). |
| $R_{bat,est}$ | Estimated R_{bat} (Ω). |
| \vec{Z}_{in} | Input impedance Vector. |
| Z_1, Z_2 | Impedance of primary and secondary coil (Ω). |
| T_v | Voltage conversion ratio of V_2/V_1 . |
| A_1, A_2 | Amplifier for peak detection and voltage follower of peak detection circuit. |
| R_i, R_f | Input resistance of A_1 and feedback loop resistance of peak detection circuit (Ω). |
| D_f, D_o | Feedback loop diode and rectification diode of peak detection circuit. |
| C_o, R_o | Output capacitor and resistance of peak detection circuit (F), (Ω). |
| V_s, V_o | Output voltage of current sensor and voltage of C_o (V). |
| V_{out} | Output voltage of A_2 (V). |
| $I_{1,o}, I_{1,a}$ | Peak current of transmitter coil at $f = f_0$ and $f = f_a$ (A). |
| $V_{1,o}, V_{1,a}$ | Peak voltage of transmitter coil at $f = f_0$ and $f = f_a$ (V). |
| $\left \vec{Z}_{in,o} \right , \left \vec{Z}_{in,a} \right $ | Magnitude of input impedance vector at $f = f_0$ and $f = f_a$. |
| $R_{L,eq,est}, M_{12,est}$ | Estimated R_L and M_{12} (Ω), (H). |
| $I_{bat,est}, V_{bat,est}$ | Estimated I_{bat} and V_{bat} (A), (V). |
| I_{end} | End charging current (A). |
| I_{ref} | Charging current reference (A). |
| f_{CV1}, f_{CV2} | f for CV operation (Hz). |
| h, v | Coil alignment change in axial and radial direction of coil (cm). |
| L_{dev} | Deviated inductance according to alignment of coil (H). |

| | |
|---|--|
| $\left \vec{Z}_{in,a,measure} \right $ | Measured value of $\left \vec{Z}_{in,a} \right $ at $f = f_a$. |
| $\left \vec{Z}_{in,o,measure} \right $ | Measured value of $\left \vec{Z}_{in,o} \right $ at $f = f_o$. |
| $R_{bat,est,dev}$ | Estimated R_{bat} in L_{dev} (Ω). |
| $R_{bat,est,fa}, R_{bat,est,fo}$ | Estimated R_{bat} by using $\left \vec{Z}_{in,a,measure} \right $ and $\left \vec{Z}_{in,o,measure} \right $ (Ω). |
| $M_{12,est,dev}$ | Estimated M_{12} in L_{dev} (H). |
| $M_{12,est,fa}, M_{12,est,fo}$ | Estimated M_{12} by using $\left \vec{Z}_{in,a,measure} \right $ and $\left \vec{Z}_{in,o,measure} \right $ (H). |

References

1. Marco, D.D.; Dolar, A.; Longo, M. A review on dynamic wireless charging systems. In Proceedings of the IEEE Milan PowerTech, Milan, Italy, 23–27 June 2019.
2. Dolar, A.; Leva, S.; Longo, M.; Dezza, F.C.; Mauri, M. Coil design and magnetic shielding of a resonant wireless power transfer system for electric vehicle battery charging. In Proceedings of the IEEE 6th International Conference on Renewable Energy Research and Applications (ICRERA), San Diego, CA, USA, 5–8 November 2017; pp. 200–205.
3. Shin, J.; Shin, S.; Kim, Y.; Ahn, S.; Lee, S.; Jung, G.; Jeon, S.J.; Cho, D.H. Design and implementation of shaped magnetic-resonance-based wireless power transfer system for roadway-powered moving electric vehicles. *IEEE Trans. Ind. Electron.* **2015**, *61*, 1179–1192. [[CrossRef](#)]
4. Silay, K.M.; Dehollain, C.; Declercq, M. Inductive power link for a wireless cortical implant with biocompatible packaging. In Proceedings of the IEEE SENSORS Conference, Kona, HI, USA, 1–4 November 2010; pp. 94–98.
5. Stielau, O.H.; Covic, G.A. Design of loosely coupled inductive power transfer systems. In Proceedings of the International Conference on Power System Technology, Perth, Australia, 4–7 December 2000; pp. 85–90.
6. Wang, C.S.; Stielau, O.H.; Covic, G.A. Design considerations for a contactless electric vehicle battery charger. *IEEE Trans. Ind. Electron.* **2005**, *52*, 1308–1314. [[CrossRef](#)]
7. Chopra, S.; Bauer, P. Analysis and design considerations for a contactless power transfer system. In Proceedings of the 33rd International Telecommunications Energy Conference (INTELEC), Amsterdam, The Netherlands, 9–13 October 2011; pp. 1–6.
8. Bosshard, R.; Kolar, J.W.; Mühlethaler, J.; Stevanović, I.; Wunsch, B.; Canales, F. Modeling and η - α -pareto optimization of inductive power transfer coils for electric vehicles. *IEEE J. Emerg. Sel. Top. Power Electron.* **2015**, *3*, 50–64. [[CrossRef](#)]
9. Zheng, C.; Lai, J.S.; Chen, R.; Faraci, W.E.; Zahid, Z.U.; Gu, B.; Zhang, L.; Lisi, G.; Anderson, D. High-efficiency contactless power transfer system for electric vehicle battery charging application. *IEEE J. Emerg. Sel. Top. Power Electron.* **2015**, *3*, 65–74. [[CrossRef](#)]
10. Tran, D.H.; Vu, V.B.; Choi, W. Design of a high-efficiency wireless power transfer system with intermediate coils for the on-board chargers of electric vehicles. *IEEE Trans. Power Electron.* **2018**, *33*, 175–187. [[CrossRef](#)]
11. Qu, X.; Han, H.; Wong, S.C.; Tse, C.K.; Chen, W. Hybrid IPT topologies with constant current or constant voltage output for battery charging applications. *IEEE Trans. Power Electron.* **2015**, *30*, 6329–6337. [[CrossRef](#)]
12. Mai, R.; Chen, Y.; Li, Y.; Zhang, Y.; Cao, G.; He, Z. Inductive power transfer for massive electric bicycles charging based on hybrid topology switching with a single inverter. *IEEE Trans. Power Electron.* **2017**, *32*, 5897–5906. [[CrossRef](#)]
13. Li, S.; Mi, C.C. Wireless power transfer for electric vehicle application. *IEEE J. Emerg. Sel. Top. Power Electron.* **2015**, *3*, 4–17.
14. Song, K.; Li, Z.; Jiang, J.; Zhu, C. Constant current/voltage charging operation for series-series and series-parallel compensated wireless power transfer systems employing primary-side controller. *IEEE Trans. Power Electron.* **2018**, *33*, 8065–8080. [[CrossRef](#)]
15. Yin, J.; Lee, C.K.; Parisini, T.; Hui, S.Y. Front-End Monitoring of Multiple Loads in Wireless Power Transfer Systems without Wireless Communication Systems. *IEEE Trans. Power Electron.* **2016**, *31*, 2510–2517. [[CrossRef](#)]
16. Yin, J.; Lee, C.K.; Hui, S.Y. A systematic approach for load monitoring and power control in wireless power transfer systems without any direct output measurement. *IEEE Trans. Power Electron.* **2015**, *30*, 1657–1667. [[CrossRef](#)]

17. Su, Y.G.; Zhang, Y.H.; Wang, Z.H.; Hu, A.P.; Chen, L.; Sun, Y. Steady-state load identification method of inductive power transfer system based on switching capacitors. *IEEE Trans. Power Electron.* **2015**, *30*, 6349–6355. [[CrossRef](#)]
18. Yin, J.; Parisini, T.; Hui, S.Y. Front-end monitoring of the mutual inductance and load resistance in a series-series compensated wireless power transfer system. *IEEE Trans. Power Electron.* **2016**, *31*, 7339–7352. [[CrossRef](#)]
19. Wang, Z.H.; Li, Y.P.; Tang, C.S.; Lv, X. Load detection model of voltage-fed inductive power transfer system. *IEEE Trans. Power Electron.* **2013**, *28*, 5233–5243. [[CrossRef](#)]
20. Sedra, S.; Smith, K.C. *Microelectronic Circuits*, 5th ed.; Oxford University Press: Oxford, UK, 1998.



© 2019 by the authors. Licensee MDPI, Basel, Switzerland. This article is an open access article distributed under the terms and conditions of the Creative Commons Attribution (CC BY) license (<http://creativecommons.org/licenses/by/4.0/>).